NANO · MICRO small
www.small-journal.com

Efficient Suppression of Dendrites and Side Reactions by Strong Electrostatic Shielding Effect via the Additive of Rb_2SO_4 for Anodes in Aqueous Zinc-Ion Batteries

Xiaoqin Zhang, Ji Chen, Heng Cao, Xiaomin Huang, Yu Liu, Yuxiang Chen, Yu Huo, Dunmin Lin, Qiaoji Zheng,* and Kwok-ho Lam**

Aqueous zinc-ion batteries (AZIBs) have attracted considerable attention due to their low cost and environmental friendliness. However, the rampant dendrite growth and severe side reactions during plating/stripping on the surface of zinc (Zn) anode hinder the practicability of AZIBs. Herein, an effective and non-toxic cationic electrolyte additive of Rb_2SO_4 is proposed to address the issues. The large cation of Rb^+ is preferentially adsorbed on the surface of Zn metal to induce a strong shielding effect for realizing the lateral deposition of Zn^{2+} ions along the Zn surface and isolating water from Zn metal to effectively inhibit side reactions. Consequently, the Zn||Zn symmetric cell with the addition of 1.5 mM Rb_2SO_4 can cycle more than 6000 h at 0.5 mA cm^{-2}/0.25 mAh cm^{-2}, which is 20 times longer than that without Rb_2SO_4. Besides, the Zn||Cu asymmetric cell with Rb_2SO_4 achieves a very high average Coulombic efficiency of 99.16% up to 500 cycles. Moreover, the electrolyte with Rb_2SO_4 well matches with the VO_2 cathode, achieving high initial capacity of 412.7 mAh g^{-1} at 5 A g^{-1} and excellent cycling stability with a capacity retention of 71.6% at 5 A g^{-1} after 500 cycles for the Zn//VO_2 full cell.

1. Introduction

In recent years, aqueous zinc-ion batteries (AZIBs) are of interest for their low redox potential, high energy density (820 mAh g^{-1} and 5855 mAh cm^{-3}), intrinsic safety, and environmental friendliness.[1–6] However, for zinc (Zn) metal anodes, Zn dendrites and side reactions of hydrogen evolution and corrosion during chemical reactions significantly degrade the cycling properties, plating/stripping Coulombic efficiency (CE), and safety of the batteries, hindering the commercialization of AZIBs.[7–9] It is critical to develop highly reversible dendrite-free and anti-side-reaction Zn metal anodes for the practicality of AZIBs.

Recently, various strategies have been proposed to extend the cycle life of AZIBs by addressing the problems of Zn dendrites, hydrogen evolution, and corrosion on the anodes, including the construction of artificial interface layer,[10–14] the structure and morphology optimization of Zn metal[15–17] and the design of electrolyte additives.[18–24] Among them, the strategy of electrolyte additive is most favored because of the excellent operability/reproducibility/diversity and cost effectiveness.[25–27] At present, common additives are mainly divided into organic small molecules, organic solvents, and inorganic molecules.[28–30] For example, Cao et al. introduced dimethyl sulfoxide to $ZnCl_2$-H_2O aqueous electrolytes to significantly inhibit hydrogen evolution and Zn dendrite growth, exhibiting the cycle life of 1000 h at a current density of 0.5 mA cm^{-2} and a capacity of 0.5 mAh cm^{-2}.[19] Li et al. found that the reversibility of Zn metal anode could be greatly enhanced after the addition of *N*-methyl-2-pyrrolidone into dilute electrolytes, giving the cycle life of 540 h at a current density of 1 mA cm^{-2} with the capacity of 1 mAh cm^{-2}.[31] Dai et al. added a small amount of $NiSO_4$ to the 2 M $ZnSO_4$ solution such that the optimized cell operates for over 900 h at 1 mA cm^{-2}.[32] Obviously, compared to organic additives, inorganic compounds have better compatibility with aqueous electrolytes. On the other hand, it has been reported that the electrolyte additives containing alkali metal ion of Na^+ or K^+ can effectively suppress Zn dendrites and mitigate side reactions during plating/stripping by a electrostatic shielding effect, for example, the Zn||Zn symmetric cell with sodium sulfate additive has good cycling stability over 300 h at a current density of 0.2 mA cm^{-2} and the cells cycled with K_2SO_4 additive show the stability

X. Zhang, J. Chen, H. Cao, X. Huang, Y. Liu, Y. Chen, Y. Huo, D. Lin, Q. Zheng
College of Chemistry and Materials Science
Sichuan Normal University
Chengdu 610066, China
E-mail: ddmd222@sicnu.edu.cn; joyce@sicnu.edu.cn
K.-ho Lam
Centre for Medical and Industrial Ultrasonics
James Watt School of Engineering
University of Glasgow
Glasgow, Scotland G12 8QQ, United Kingdom
E-mail: kwokho.lam@glasgow.ac.uk

The ORCID identification number(s) for the author(s) of this article can be found under https://doi.org/10.1002/smll.202303906

DOI: 10.1002/smll.202303906

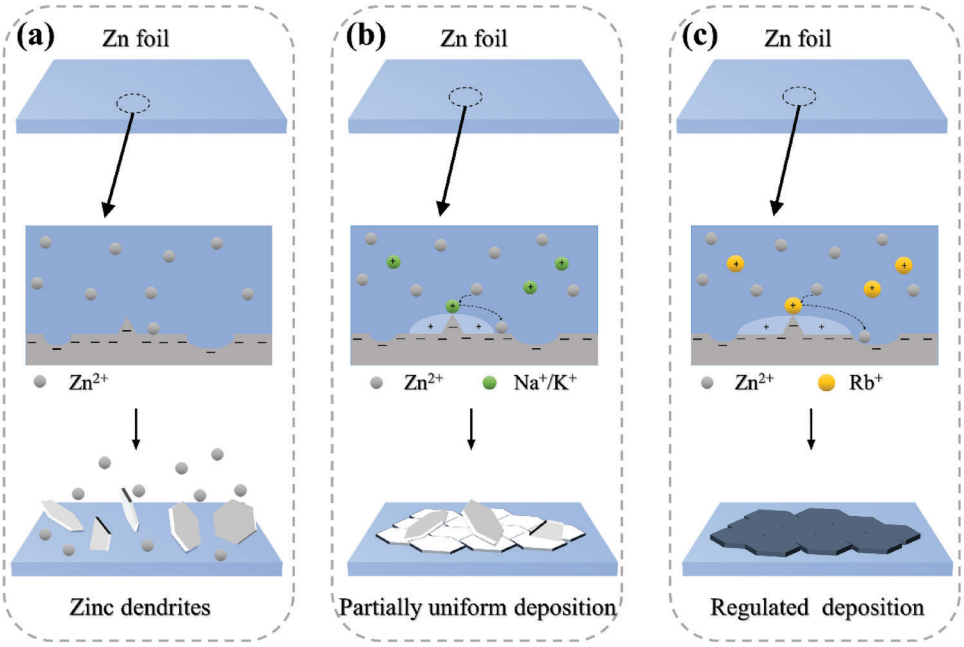

Figure 1. Schematic diagram of Zn deposition cycled in a) $ZnSO_4$ (2 M), b) $ZnSO_4$ (2 M) +1.5 mM Na_2SO_4/K_2SO_4, and c) $ZnSO_4$ (2 M) + 1.5 mM Rb_2SO_4 electrolytes.

of more than 3500 h at 0.5 mA cm^{-2}.[20,33] However, to our knowledge, there have been no reports about the electrolyte additives containing Rb^+ (1.52 Å) with a larger radius than Na^+ (1.02 Å) or K^+ (1.38 Å) ions.[34] It is reasonably anticipated that Rb^+ may be more efficient to occupy the tip of the Zn surface and induce a larger electrostatic shielding area due to its larger radius and spatial potential resistance than Na^+ or K^+, prompting the lateral deposition of Zn^{2+} along the Zn metal surface.

Herein, a simple electrolyte additive of Rb_2SO_4 has been developed to optimize the $ZnSO_4$ electrolyte for suppressing Zn dendrites and side reactions during plating/stripping. It is found that large Rb^+ can be more easily adsorbed on the surface of Zn metal than H_2O due to its much larger adsorption energy, inducing a larger electrostatic shielding area to homogenize the deposition of Zn^{2+} ions along the Zn surface and simultaneously isolating water from Zn metal to regulate the anode-electrolyte interface for mitigating side reactions. Consequently, the addition of the Rb_2SO_4 significantly enhances the ability of Zn metal to inhibit side reactions, more importantly, the cycling life of the Zn metal anode is greatly lengthened: the Zn||Zn symmetric cell with the addition of 1.5 mM Rb_2SO_4 possesses a much longer cycling life of more than 6000 h at 0.5 mA cm^{-2}/0.25 mAh cm^{-2}, which is 20 times longer than that of the Zn||Zn symmetric cell without the addition of Rb_2SO_4 (300 h).

2. Results and Discussion

A schematic diagram of Zn^{2+} plating in various electrolytes is exhibited in **Figure 1**. As shown in Figure 1a, the surface of common commercial Zn foil is not smooth with scratches and pits, resulting in the uneven distribution of the negative electric field on the surface of the Zn foil. In $ZnSO_4$ electrolyte, Zn^{2+} ions are preferentially deposited on the protrusions of the Zn foil due to the "tip effect," which induces the uneven distribution of the negative electric field, leading to Zn dendrite growth and side reactions.[35] In contrast, in $ZnSO_4$+Na_2SO_4/K_2SO_4 electrolyte, as shown in Figure 1b, Na^+/K^+ may be preferentially adsorbed at the protrusions of the Zn foil, acting as an electrostatic shield to realize the lateral deposition of Zn^{2+} ions along the surface of Zn foil. As shown in Figure 1c, compared with Na^+/K^+, Rb^+ has larger volume and spatial potential resistance, leading to a more significant electrostatic shielding area and inducing a more effective separation layer between water and Zn foil to inhibit Zn dendrites and side reactions.

The ability of anticorrosion of the Zn metal anode is evaluated by immersing the Zn metal anode into various Zn sulfate electrolytes with or without the additives for 5 days, and the results are shown in **Figure 2**a,b and Figure S1, Supporting Information. In Figure 2a, after soaked for 5 days in the $ZnSO_4$ without the additive, numerous sharp ultra-thin nanosheets with larger dimensions are grown obliquely on the surface of Zn foil. However, in the $ZnSO_4$ with Na_2SO_4, a large number of small-size nanosheets and a small number of large-size nanosheets are grown simultaneously on the surface of the soaked Zn foil for 5 days (Figure S1a, Supporting Information), while in the $ZnSO_4$ with K_2SO_4, the nanoflakes on the surface of the soaked Zn foil become quite small (Figure S1b, Supporting Information), suggesting that the corrosion resistance of the Zn foil is gradually improved with the addition of Na_2SO_4 or K_2SO_4. More interestingly, as shown in Figure 2b, the Zn foil soaked in the $ZnSO_4$ electrolyte with Rb_2SO_4 exhibits much superior corrosion resistance. The surface of the Zn foil remains relatively flat and smooth with a very small number of cracks and holes after being immersed in the $ZnSO_4$ electrolyte with Rb_2SO_4 for 5 days, suggesting a very weak corrosion behavior. As shown in Figure S2, Supporting Information, strong characteristic diffraction peaks of Zn hydroxide

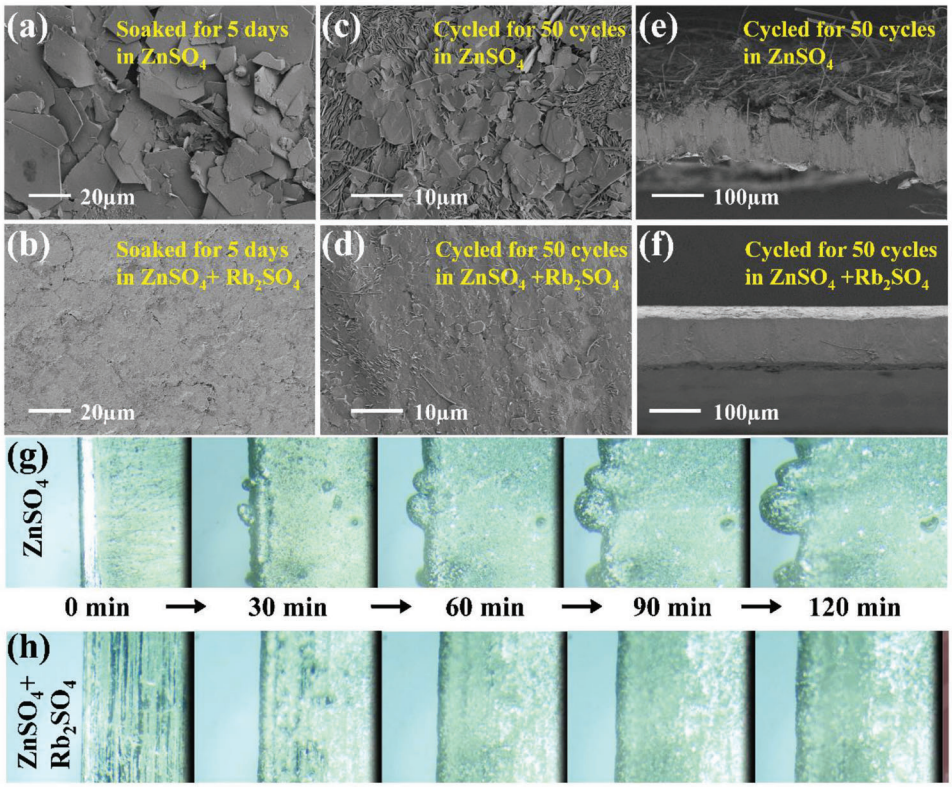

Figure 2. SEM images of Zn soaked for 5 days in a) $ZnSO_4$ (2 M) and b) $ZnSO_4$ (2 M) +1.5 mM Rb_2SO_4 electrolytes. SEM images of Zn metal anodes cycled for 50 cycles in c) $ZnSO_4$ (2 M) and d) $ZnSO_4$ (2 M) + 1.5 mM Rb_2SO_4 electrolytes at a current density of 1 mA cm^{-2} and a capacity of 1 mAh cm^{-2}, and e,f) cross-sectional SEM images of Zn metal anodes cycled for 50 cycles in $ZnSO_4$ (2 M) without/with 1.5 mM Rb_2SO_4 additive. In situ optical microscopic images of Zn^{2+} deposition on Zn foils at a current density of 20 mA cm^{-2} in g) $ZnSO_4$ (2 M) and h) $ZnSO_4$ (2 M) + 1.5 mM Rb_2SO_4 electrolytes. (Zn foil thickness: 100 μm).

hydrate by-product ($Zn_4SO_4(OH)_6{\cdot}5H_2O$, PDF#39-0688) are detected for the soaked Zn foil for 5 days in the $ZnSO_4$ electrolyte, but no diffraction peaks of by-products are observed in the XRD pattern of the soaked Zn foil for 5 days in the $ZnSO_4$ electrolyte with Rb_2SO_4. Likewise, the elemental distribution mappings in Figures S3 and S4, Supporting Information also exhibit that large amounts of oxygen and sulfur elements are detected for the Zn foil immersed in the $ZnSO_4$ electrolyte without Rb_2SO_4 (Figure S3, Supporting Information), while no significant O and S elements are found for the Zn foil soaked in the $ZnSO_4$ electrolyte with Rb_2SO_4 (Figure S4, Supporting Information). All of the above results confirm that the additive of Rb_2SO_4 can effectively inhibit side reactions at the interface between the anode and the electrolyte. The SEM images of the Zn foils cycled for 50 cycles at 1 mA cm^{-2} and 1 mAh cm^{-2} in the $ZnSO_4$ electrolytes without/with Na_2SO_4, K_2SO_4, or Rb_2SO_4 are shown in Figure 2c–d and Figure S5, Supporting Information. In Figure 2c, numerous sharp nanoflakes composed of the $Zn_4SO_4(OH)_6{\cdot}5H_2O$ byproduct are grown on the surface of the Zn foil cycled for 50 cycles in the $ZnSO_4$ electrolyte, indicating severe Zn dendrite growth and side reactions during plating/stripping. Fortunately, after the introduction of Na_2SO_4, K_2SO_4, or Rb_2SO_4 into the $ZnSO_4$ electrolyte, the number of nanoflakes is significantly reduced on the surface of the Zn foil cycled for 50 cycles (Figure 2c–f; Figures S5 and S6, Supporting Information), indicating that the Zn dendrite and side reactions are greatly suppressed. Especially, the Zn foil cycled in the $ZnSO_4$ electrolyte with Rb_2SO_4 possesses a smooth and dense surface, showing no large dendrites (Figure 2d) and characteristic diffraction peaks of $Zn_4SO_4(OH)_6{\cdot}5H_{2O}$ byproduct (Figure S6, Supporting Information). Similarly, the cross-sectional SEM images of Zn metal anodes cycled for 50 cycles in the $ZnSO_4$ electrolyte without/with Rb_2SO_4 show that numerous random dendrites are formed on the surface of the Zn foil cycled for 50 cycles in the $ZnSO_4$ electrolyte without Rb_2SO_4 (Figure 2e), but the Zn foil in the $ZnSO_4$ electrolyte with Rb_2SO_4 exhibits a smooth and flat surface with the obvious formation of dendrites (Figure 2f), which is similar to the original Zn foil (Figure S7, Supporting Information). Based on the above results, the side reactions between the electrolyte and the Zn foil can be expressed as follows.

$$Zn \leftrightarrow Zn^{2+} + 2e^- \quad (1)$$

$$2H_2O + 2e^- \leftrightarrow H_2 + 2OH^- \quad (2)$$

$$4Zn^{2+} + 6OH^- + 4SO_4^{2-} + 5H_2O \leftrightarrow Zn_4SO_4(OH)_6 \cdot 5H_2O \quad (3)$$

To intuitively evaluate the inhibition of additives on Zn dendrites, the electrochemical deposition behavior of Zn^{2+} is observed in situ at 20 mA cm^{-2} in various $ZnSO_4$ electrolytes via

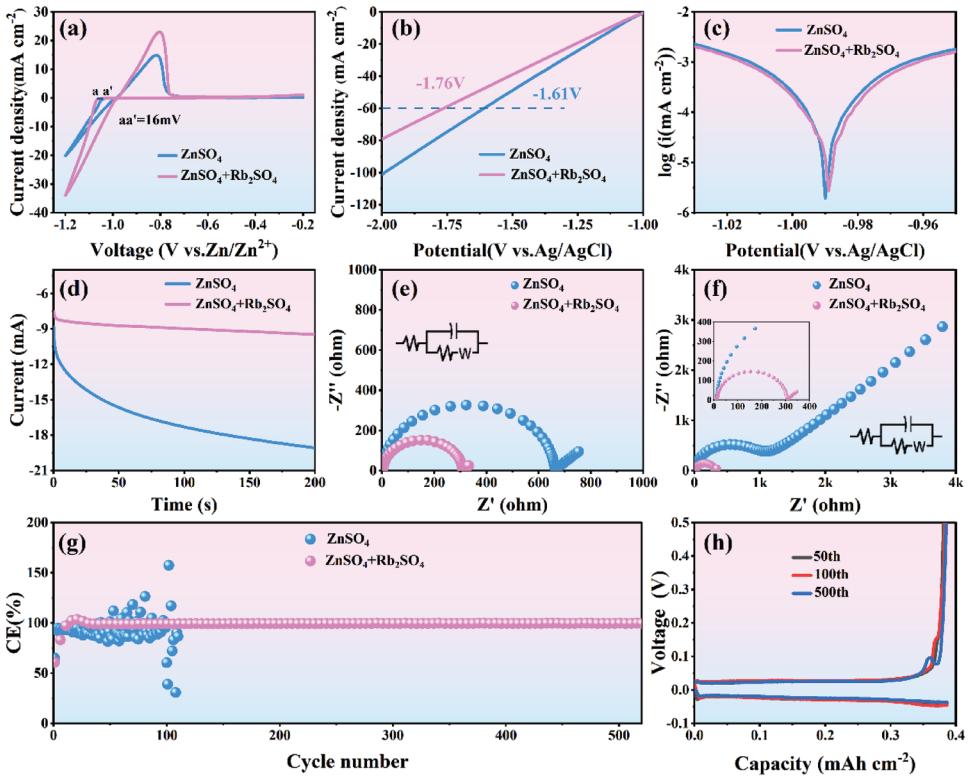

Figure 3. a) Nucleation overpotentials of Zn ions for Zn||Ti asymmetric cells at 1 mV s^{-1} in $ZnSO_4$ (2 M) and $ZnSO_4$ (2 M) + 1.5 mM Rb_2SO_4 electrolytes. b) LSV curves (HER) and c) Tafel curves of Zn electrodes at a scan rate of 1 mV s^{-1} in $ZnSO_4$ (2 M) and $ZnSO_4$ (2 M) + 1.5 mM Rb_2SO_4 electrolytes. d) CA curve of Zn plate in ZnSO4 electrolyte with/without 1.5 mM Rb_2SO_4 additive at −150 mV. Electrochemical impedance spectra of Zn||Zn symmetric cells in $ZnSO_4$ and $ZnSO_4$ (2 M) + 1.5 mM Rb_2SO_4 electrolytes e) before cycling and f) after 50 cycles. g) CE of Zn||Cu cells in 2 M $ZnSO_4$ with and without 1.5 mM Rb_2SO_4 (0.5 mA cm^{-2}) and h) corresponding voltage curves at different cycles in the electrolyte of $ZnSO_4$ (2 M) + 1.5 mM Rb_2SO_4. (Zn foil thickness: 100 µm).

optical microscopy and the results are presented in Figure 2g,h; Figure S8 and Videos S1–S4, Supporting Information). As shown in Figure 2g, in the $ZnSO_4$ electrolyte without additive, obvious protrusions are observed on the surface of the Zn foil after Zn plating for 30 min, and numerous dendrites become larger with time increasing (Video S1, Supporting Information). However, as shown in Figure 2h; Figure S8 and Videos S2–S4, Supporting Information, the addition of the additive (Na_2SO_4, K_2SO_4, or Rb_2SO_4) into the $ZnSO_4$ electrolyte successfully inhibits the growth of dendrites during Zn plating. Compared with the Zn foil electrically cycled in the $ZnSO_4$ electrolyte without additive, much smaller and fewer dendrites are observed on the surfaces of the Zn foils cycled in the $ZnSO_4$ electrolytes with additives, and their surfaces are much smoother (Figure 2h; Figure S8 and Videos S2–S4, Supporting Information), suggesting the critical role of additives on uniform deposition behaviors. More importantly, in the $ZnSO_4$ electrolyte containing 1.5 mmol L^{-1} Rb_2SO_4, no significant protrusions are observed and the surface is still very smooth for the Zn foil plated for 120 min (Figure 2h), indicating the excellent inhibition on Zn dendrites induced by Rb_2SO_4 (Video S4, Supporting Information).

The nucleation overpotentials of Zn metals in the $ZnSO_4$ (2 M) electrolytes with/without Rb_2SO_4 are shown in **Figure 3**a. Compared with that in the $ZnSO_4$ electrolyte, the Zn nucleation overpotential in the Rb^+-containing $ZnSO_4$ electrolyte is increased by 16 mV (Figure 3a), leading to stronger nucleation driving force and the formation of tiny Zn nuclei, which favors the preferred nucleation orientation growth and thus prohibits the random 2D diffusion of Zn^{2+} as well as avoids the "tip effect."[36] The LSV curves and Tafel curves of Zn foils in the $ZnSO_4$ and $ZnSO_4$ + Rb_2SO_4 electrolytes are shown in Figure 2b, Figure S9, Supporting Information, and Figure 2c. In the $ZnSO_4$ electrolyte, the potential of the Zn foil for hydrogen evolution reaction (HER) is −1.61 V (versus Ag/AgCl) at a current density of 60 mA cm^{-2} and shows a significant current response in the subsequent negative scan (Figure 3b). From Figure S9, Supporting Information, the addition of Rb^+ simultaneously suppresses the H_2 and O_2 evolution reactions.[37,38] In contrast, the potential of the Zn metal for HER in the Rb^+-containing electrolyte is increased by 150 mV, implying a better inhibition of H_2 reduction by Rb ions.[12,39] In addition, the corrosion potential (−0.989 V) of the electrode in the electrolyte with Rb ions is much higher than that of the electrode in the $ZnSO_4$ electrolyte (−0.990 V), as shown in Figure 3c, indicating the improved corrosion resistance of Zn foil after the addition of Rb_2SO_4. The potentiostatic current time transient curves of Zn foils in different electrolytes are shown in Figure 3d. The mechanism of different deposition behaviors of Zn^{2+} in various electrolytes is further investigated by chronoamperometry (CA) (Figure 3d). It can be seen that when a constant overpotential

of −150 mV is applied to the Zn electrode in the $ZnSO_4$ electrolyte, the current density continues to increase for more than 200 s, indicating a continuous 2D diffusion process, which is unfavorable to the uniform nucleation of Zn^{2+}. In contrast, for the Zn electrode in the $ZnSO_4$ electrolyte with Rb^+, the current density hardly increases after 5 s, showing that the Zn foil in the Rb^+-containing electrolytes exhibits initial Zn nucleation and 2D diffusion within only 5 s and then possesses a stable 3D diffusion process,[40] which is significantly beneficial for the uniform nucleation of Zn^{2+} and thus lead to a uniform Zn plating layer. The electrochemical impedance spectra of the Zn||Zn symmetric cells in the $ZnSO_4$ electrolytes without/with Rb_2SO_4 before and after cycling are exhibited in Figure 3e,f. As shown in Figure 3f, the charge transfer resistance of the cell with the Rb^+-containing $ZnSO_4$ electrolyte is much lower than that of the cell with the $ZnSO_4$ electrolyte without Rb^+ (Figure 3e), indicating enhanced reaction kinetics induced by the additive of Rb_2SO_4. For the cell with the Rb^+-containing $ZnSO_4$ electrolyte, there has been no significant change in the charge transfer resistance before and after 50 cycles (Figure 3f). However, for the cell with the $ZnSO_4$ electrolyte without Rb^+, the charge transfer resistance is greatly increased after 50 cycles, which is attributed to the generation of $Zn_4SO_4(OH)_6{\cdot}5H_2O$ byproduct. Clearly, the introduction of Rb^+ effectively reduces the anodic interfacial resistance with less passivation of the Zn electrode, fastening charge transfer during charging and discharging.[41] The CEs of the Zn||Cu asymmetric cells in the 2 M $ZnSO_4$ without/with 1.5 mM Rb_2SO_4 are shown in Figure 3g,h and Figure S10, Supporting Information. As shown in Figure 3g and Figure S10, Supporting Information, the cell with the pristine $ZnSO_4$ electrolyte is cycled unsteadily with an initial CE of 65.2%, and then fails after 110 h. However, for the cell with the Rb^+-added $ZnSO_4$ electrolyte, a much higher initial CE of 75.3% is exhibited and an excellent average CE of 99.16% is achieved for 500 cycles (Figure 3g,h). The Zn||Cu batteries have a voltage peak at ≈0.35 V with a gradually enhanced intensity in the charge and discharge curves, which is caused by the alloying process of Zn on a Cu substrate (Figure 3h). This Zn-Cu alloy phase may provide abundant active sites for the uniform deposition of Zn ions, extending the cycle life of the cell.[42]

The Zn||Zn symmetric cells are assembled to evaluate the effect of the type and concentration of the additives on the electrochemical cycling stability and rate performance at different current densities and the results are provided in **Figure 4**a and Figure S11–S14, Supporting Information. As shown in Figure S11, Supporting Information, for the cells in the $ZnSO_4$ electrolytes without the additive and with Na_2SO_4, K_2SO_4, and Rb_2SO_4, the cycle times of 160, 220, 780 h, and more than 1300 h are achieved, respectively, suggesting a very strong positive effect of the additive of Rb_2SO_4 on the cycle life of the Zn||Zn symmetric cell. In addition, as shown in Figure S12, Supporting Information, the concentration of Rb_2SO_4 plays a critical role in improving the cycle life of the Zn||Zn symmetric cell. The optimal cycle life of more than 1300 h is achieved at the concentration of 1.5 mM Rb_2SO_4. In Figure 4a, at 0.5 mA cm^{-2}/0.25 mAh cm^{-2}, the Zn||Zn symmetric cell in the $ZnSO_4$ electrolyte with Rb_2SO_4 possesses an amazing cycle life of more than 6000 h that is 20 times longer than that in the $ZnSO_4$ electrolyte. To better demonstrate the effect of Rb^+ on the suppression of dendrites, the cycling tests of symmetric cells are performed and shown in Figure S13, Supporting Information using thin Zn foils (thickness: 20 μm) at high current densities. Clearly, the cells cycled in $ZnSO_4$ electrolyte with 1.5 mM Rb_2SO_4 are much more stable than others without Rb^+ addition and with other Rb^+ concentrations under the depth of discharge (DOD) of 42.78%. Figures S12 and S13, Supporting Information show that the optimum concentration of Rb_2SO_4 is 1.5 mM. When the concentration of Rb^+ added is too low, the tip of Zn anode may not be fully occupied, causing a weak tip effect that leads to dendrites and side reactions. On the other hand, when the level of Rb^+ is too high, Rb^+ may occupy more active sites on the surface of Zn to induce the excessive electrostatic shielding effect, which is not conducive to the uniform deposition of Zn ions. In Figure S14, Supporting Information, when the current density increases from 0.5 to 5 mA cm^{-2}, the cycle life of the cell in the $ZnSO_4$ electrolyte with the addition of Rb^+ is more than 100 h, but the cell in the $ZnSO_4$ electrolyte is out of order after 80 h, indicating that the cell is short-circuited due to the dendrite penetrating the separation. As shown in Figure S15, Supporting Information, we performed FT-IR tests on the electrolytes without and with Rb^+, where the broad peak (2900–3700 cm^{-1}) can be attributed to the O—H stretching vibration of H_2O molecules, the peak (1600–1700 cm^{-1}) comes from the bending vibration of H_2O molecules and the peak at around 1100 cm^{-1} can be ascribed to the stretching vibration of SO_4^{2-}. It can be seen that the position and intensities of the three peaks do not change after the addition of Rb^+, which verifies that the solvation structure of the electrolyte remains unchanged.[43] To investigate the phenomena theoretically, the density function theory (DFT) is used to calculate the adsorption energy of Rb^+ and H_2O on the Zn (002) crystal plane of Zn metal to reveal the inhibition principle of the additive of Rb_2SO_4 on Zn dendrites and side reactions. As shown in Figure 4b,c, the adsorption energy between Rb^+ and Zn metal is −32.60 kcal mol^{-1}, which is much larger than that between H_2O molecules and Zn metal (−3.55 kcal mol^{-1}). The calculated parameters are shown in Figure S16, Supporting Information. Due to the much larger adsorption energy compared to water, Rb^+ may be adsorbed on the surface of Zn metal more preferentially, leading to a strong shielding effect for the promotion of the lateral deposition of Zn^{2+} ions along the surface of Zn metal. The electric double-layer (EDL) capacitance at Zn anode surface can also certify the Rb^+ adsorption on the Zn foil surface (Figure S17, Supporting Information). The EDL capacitance of the Rb^+-containing electrolyte (159.45 μF cm^{-2}) is remarkably lower than that of the pure 2 M $ZnSO_4$ electrolyte (216.09 μF cm^{-2}). The decrease of EDL capacitance is due to the Rb_2SO_4 additives occupying high active sites triggered by the tip effect, leading to the adsorption of Zn^{2+} to conventional surface-active sites.[44–46] In addition, numerous Rb^+ ions absorbed on the surface of Zn metal isolate water from Zn metal and thus effectively suppress side reactions during charging and discharging. As shown in Figure 4d and Table S1, Supporting Information, the electrochemical performance of the Zn||Zn symmetric cell in $ZnSO_4$ electrolyte with Rb_2SO_4 is comparable/superior to that of the reported Zn||Zn symmetric cells studied with various strategies.[19–22,26,31,32,46–54] The symmetric battery is used to cycle more than 6000 h at 0.5 mA cm^{-2}/0.25 mAh cm^{-2}, then the plating time is 3000 h, so the cumulative capacity is 0.5 mA cm^{-2} × 3000 h, and the result is 1500 mAh cm^{-2}.

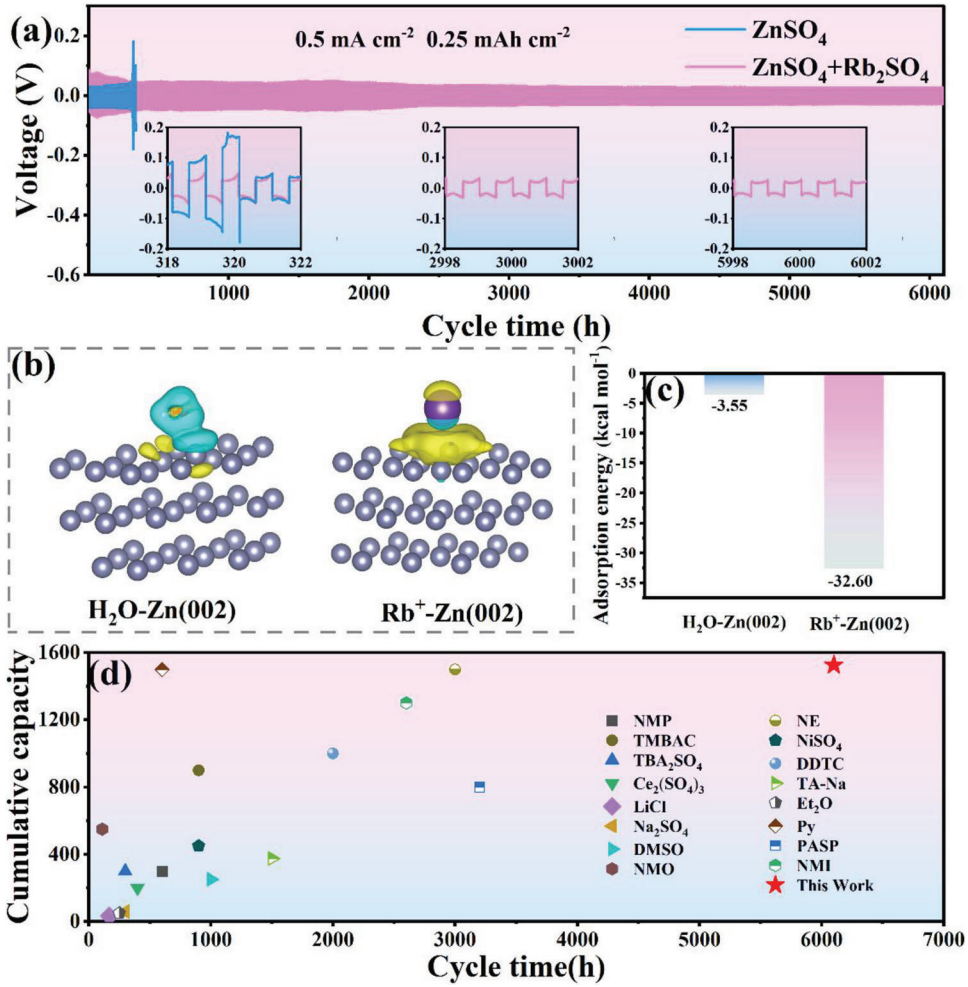

Figure 4. a) Long-term cycling performance of Zn||Zn symmetric cells in $ZnSO_4$ (2 M) electrolytes without/with 1.5 mM Rb_2SO_4 at 0.5 mA cm^{-2}/0.25 mAh cm^{-2}. b) Schematic diagram of the adsorption of H_2O and Rb^+ molecules on the Zn (002) crystal plane of Zn metal. c) Adsorption energies of H_2O and Rb^+ molecules on the Zn (002) crystal plane of Zn metal. d) Comparison of cycle time and cumulative plating capacity between Zn||Zn symmetric cell in $ZnSO_4$ (2 M) with 1.5 mM Rb_2SO_4 and other reported Zn||Zn symmetric cells.[19–22,26,31,32,46–54] (Zn foil thickness: 100 µm).

The electrochemical properties of the Zn//VO_2 full cell assembled with VO_2 nanosheets as the cathode, Zn foil as the anode, glass fiber as the diaphragm, and $ZnSO_4$ (2 M) solution without/with Rb_2SO_4 as the electrolyte are shown in **Figure 5**. The schematic diagram of the Zn//VO_2 full cell is presented in Figure 5a, while Figures S18 and S19, Supporting Information show the SEM image and XRD pattern of VO_2, indicating the successful synthesis of VO_2. As shown in Figure 5b, similar redox peaks are observed for the Zn//VO_2 full cells in $ZnSO_4$ (2 M) solution without/with Rb_2SO_4, indicating that the additive of Rb^+ does not participate in the redox reactions during charging and discharging. The rate performance of the Zn//VO_2 cells in different electrolytes is shown in Figure 5c. Clearly, the Zn//VO_2 full cell with Rb_2SO_4 possesses much better rate performance than that without Rb_2SO_4, providing high specific capacities of 371, 351, 322, 289, 248, and 156 mAh g^{-1} at 0.5, 1.0, 2.0, 3.0, 5.0, and 10 A g^{-1}, respectively. After the current density is restored to 0.5 A g^{-1}, the cell with Rb_2SO_4 provides higher specific capacities than the initial state, indicating that the additive of Rb_2SO_4 also improves the reversibility of the full cell. The EIS curves of the Zn//VO_2 full cells in different electrolytes are shown in Figure 5d. It can be clearly seen that the introduction of Rb_2SO_4 reduces the charge transfer resistance of the full cells. The charge/discharge curves in Figure 5e,f also indicate that the Zn//VO_2 full cell with Rb_2SO_4 has higher capacity retention and better cycling performance than the cell without Rb_2SO_4. The long-term cycling stabilities of the full cells are evaluated at 5 A g^{-1} and the results are shown in Figure 5g. Obviously, the addition of Rb_2SO_4 greatly improves the long-term cycling performance of the Zn//VO_2 full cell. Without Rb_2SO_4, the full cell cannot exceed 200 cycles, while the Zn//VO_2 full cell with Rb_2SO_4 can perform more than 500 cycles, giving the capacity retention of 71.6% at 5 A g^{-1} after 500 cycles. To verify the universal effect of Rb^+ on the improvement of electrochemical performance, the Zn//VO_2 full cells are assembled using a thin Zn foil as the anode and the VO_2 as the cathode. The cycling performance is shown in Figure S20, Supporting Information. The full battery with Rb^+ has a much more stable Coulomb efficiency for 800 cycles and a much better capacity retention rate than that without Rb^+. The SEM images of the Zn anodes of the full cells cycled

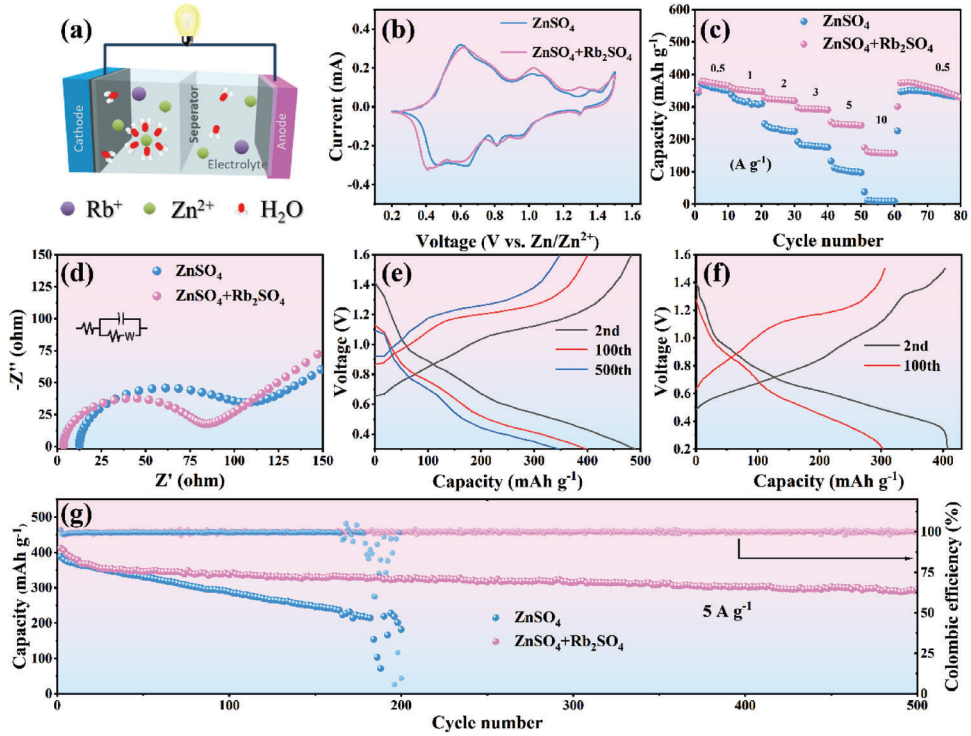

Figure 5. a) Schematic diagram of Zn//VO_2 full cell. b) Cyclic voltammograms of Zn//VO_2 full cells in different electrolytes at a scan rate of 0.1 mV s^{-1}. c) Rate capabilities of Zn//VO_2 full cells in different electrolytes at current densities from 0.5 to 10 A g^{-1}. d) EIS curves of Zn//VO_2 full cells in different electrolytes. Charge and discharge curves of Zn//VO_2 full cells in e) $ZnSO_4$ (2 M) + 1.5 mM Rb_2SO_4 and f) $ZnSO_4$ (2 M) electrolytes (5 A g^{-1}). g) Cycling performance of Zn//VO_2 full cells in different electrolytes at a current density of 5 A g^{-1}. (Zn foil thickness: 100 µm).

for 100 cycles are shown in Figure S21, Supporting Information. The Zn anode in the $ZnSO_4$+Rb_2SO_4 electrolyte still shows a very smooth surface after 100 cycles, but the anode in the $ZnSO_4$ electrolyte shows a dendritic cluster surface, showing severe dendrite growth and side reactions during the electrochemical reactions.

3. Conclusion

In summary, an electrolyte additive of Rb_2SO_4 is developed to effectively suppress the dendrite growth and side reactions on the surface of Zn metal anodes during the electrochemical reactions. It is found that large Rb^+ ions can be more preferentially adsorbed on the surface of Zn metal than water because of its much larger adsorption energy on the surface of Zn metal, providing a strong shielding effect to realize the uniform deposition of Zn^{2+} ions on the Zn surface and isolate water from Zn metal to suppress side reactions. Consequently, an excellent stability on superlong cycling of more than 6000 h is achieved for the Zn||Zn symmetric cell with the addition of 1.5 mM Rb_2SO_4 at 0.5 mA cm^{-2}/0.25 mAh cm^{-2}, which is 20 times longer than that of the Zn||Zn symmetric cell without the addition of Rb_2SO_4 (300 h). The Zn||Cu asymmetric cell with the addition of Rb_2SO_4 possesses a much higher average plating/stripping CE of 99.16% for 500 cycles than that of the Zn||Cu asymmetric cell without the addition of Rb_2SO_4. In addition, the electrolyte with Rb_2SO_4 greatly enhances the electrochemical properties of the Zn//VO_2 full cell, delivering the high initial capacity of 412.7 m Ah g^{-1} at 5 A g^{-1} and excellent cycling stability with the capacity retention of 71.6% at 5 A g^{-1} after 500 cycles. The present work proposes a feasible electrolyte optimization method to suppress Zn dendrite growth and mitigate side reactions for Zn metal anodes for AZIBs by the coregulation of interfacial electrical field and anode-electrolyte interface.

Supporting Information

Supporting Information is available from the Wiley Online Library or from the author.

Acknowledgements

This work was supported by the Natural Science Foundation of Sichuan Province (2022NSFSC0222), the Sichuan Science and Technology Program (2023NSFSC0439), and partially by the University of Glasgow. The authors also appreciate the Shiyanjia Lab (www.shiyanjia.com) for the SEM tests.

Conflict of Interest

The authors declare no conflict of interest.

Data Availability Statement

The data that support the findings of this study are available from the corresponding author upon reasonable request.

Keywords

aqueous zinc-ion batteries, electrolyte additive, side reaction, zinc dendrites

Received: May 9, 2023
Revised: July 15, 2023
Published online: August 30, 2023

[1] J. Yang, B. Yin, Y. Sun, H. Pan, W. Sun, B. Jia, S. Zhang, T. Ma, *Nano-Micro Lett.* **2022**, *13*, 79.
[2] Y. Li, Y. Liu, J. Chen, Q. Zheng, Y. Huo, F. Xie, D. Lin, *Chem. Eng. J.* **2022**, *448*, 137681.
[3] P. Ruan, S. Liang, B. Lu, H. J. Fan, J. Zhou, *Angew. Chem., Int. Ed.* **2022**, *61*, 202200598.
[4] D. Wang, Q. Li, Y. Zhao, H. Hong, H. Li, Z. Huang, G. Liang, Q. Yang, C. Zhi, *Adv. Energy Mater.* **2022**, *12*, 2102707.
[5] Y. Liu, X. Lu, F. Lai, T. Liu, P. R. Shearing, I. P. Parkin, G. He, D. J. L. Brett, *Joule* **2021**, *5*, 2845.
[6] J. Cao, D. Zhang, X. Zhang, Z. Zeng, J. Qin, Y. Huang, *Energy Environ. Sci.* **2022**, *15*, 499.
[7] Q. Zhang, J. Luan, Y. Tang, X. Ji, H. Wang, *Angew. Chem., Int. Ed.* **2020**, *59*, 13180.
[8] Z. Xing, C. Huang, Z. Hu, *Coord. Chem. Rev.* **2022**, *452*, 241299.
[9] J. Zhou, M. Xie, F. Wu, Y. Mei, Y. Hao, R. Huang, G. Wei, A. Liu, L. Li, R. Chen, *Adv. Mater.* **2021**, *33*, 2101649.
[10] S. H. Park, S. Y. Byeon, J.-H. Park, C. Kim, *ACS Energy Lett.* **2021**, *6*, 3078.
[11] P. Cao, X. Zhou, A. Wei, Q. Meng, H. Ye, W. Liu, J. Tang, J. Yang, *Adv. Funct. Mater.* **2021**, *31*, 2100398.
[12] D. Xie, Z. W. Wang, Z. Y. Gu, W. Y. Diao, F. Y. Tao, C. Liu, H. Z. Sun, X. L. Wu, J. W. Wang, J. P. Zhang, *Adv. Funct. Mater.* **2022**, *32*, 2204066.
[13] L. Kang, M. Cui, F. Jiang, Y. Gao, H. Luo, J. Liu, W. Liang, C. Zhi, *Adv. Energy Mater.* **2018**, *8*, 1801090.
[14] Y. Liu, Y. Li, X. Huang, H. Cao, Q. Zheng, Y. Huo, J. Zhao, D. Lin, B. Xu, *Small* **2022**, *18*, 2203061.
[15] Y. Zeng, X. Zhang, R. Qin, X. Liu, P. Fang, D. Zheng, Y. Tong, X. Lu, *Adv. Mater.* **2019**, *31*, 1903675.
[16] C. Li, X. Shi, S. Liang, X. Ma, M. Han, X. Wu, J. Zhou, *Chem. Eng. J.* **2020**, *379*, 122248.
[17] J. Zhou, F. Wu, Y. Mei, Y. Hao, L. Li, M. Xie, R. Chen, *Adv. Mater.* **2022**, *34*, 2200782.
[18] R. Qin, Y. Wang, M. Zhang, Y. Wang, S. Ding, A. Song, H. Yi, L. Yang, Y. Song, Y. Cui, J. Liu, Z. Wang, S. Li, Q. Zhao, F. Pan, *Nano Energy* **2021**, *80*, 105478.
[19] L. Cao, D. Li, E. Hu, J. Xu, T. Deng, L. Ma, Y. Wang, X. Q. Yang, C. Wang, *J. Am. Chem. Soc.* **2020**, *142*, 21404.
[20] Y. Xu, J. Zhu, J. Feng, Y. Wang, X. Wu, P. Ma, X. Zhang, G. Wang, X. Yan, *Energy Storage Mater.* **2021**, *38*, 299.
[21] Y. Li, P. Wu, W. Zhong, C. Xie, Y. Xie, Q. Zhang, D. Sun, Y. Tang, H. Wang, *Energy Environ. Sci.* **2021**, *14*, 5563.
[22] X. Guo, Z. Zhang, J. Li, N. Luo, G.-L. Chai, T. S. Miller, F. Lai, P. Shearing, D. J. L. Brett, D. Han, Z. Weng, G. He, I. P. Parkin, *ACS Energy Lett.* **2021**, *6*, 395.
[23] H. Cao, X. Huang, Y. Liu, Q. Hu, Q. Zheng, Y. Huo, F. Xie, J. Zhao, D. Lin, *J. Colloid Interface Sci.* **2022**, *627*, 367.
[24] H. Cao, X. Huang, Y. Li, Y. Liu, Q. Zheng, Y. Huo, R. Zhao, J. Zhao, D. Lin, *Chem. Eng. J.* **2022**, *455*, 140538.
[25] H. Jia, Z. Wang, B. Tawiah, Y. Wang, C.-Y. Chan, B. Fei, F. Pan, *Nano Energy* **2020**, *70*, 104523.
[26] A. Bayaguud, X. Luo, Y. Fu, C. Zhu, *ACS Energy Lett.* **2020**, *5*, 3012.
[27] Q. Zhang, Y. Ma, Y. Lu, Y. Ni, L. Lin, Z. Hao, Z. Yan, Q. Zhao, J. Chen, *J. Am. Chem. Soc.* **2022**, *18435*, 18435.
[28] H. Yan, X. Zhang, Z. Yang, M. Xia, C. Xu, Y. Liu, H. Yu, L. Zhang, J. Shu, *Coord. Chem. Rev.* **2022**, *452*, 241297.
[29] K. Zhao, G. Fan, J. Liu, F. Liu, J. Li, X. Zhou, Y. Ni, M. Yu, Y. M. Zhang, H. Su, Q. Liu, F. Cheng, *J. Am. Chem. Soc.* **2022**, *144*, 11129.
[30] C. Meng, W. He, L. Jiang, Y. Huang, J. Zhang, H. Liu, J. Wang, *Adv. Energy Mater.* **2022**, *32*, 2207732.
[31] T. C. Li, Y. Lim, X. L. Li, S. Luo, C. Lin, D. Fang, S. Xia, Y. Wang, H. Y. Yang, *Adv. Energy Mater.* **2022**, *12*, 2103231.
[32] Y. Dai, C. Zhang, W. Zhang, L. Cui, C. Ye, X. Hong, J. Li, R. Chen, W. Zong, X. Gao, *Angew. Chem., Int. Ed.* **2023**, *62*, e202301192.
[33] K. Han, Z. Wang, F. An, Y. Liu, X. Qu, J. Xue, P. Li, *ACS Appl. Mater. Interfaces* **2022**, *14*, 4316.
[34] Y. Sugiura, Y. Saito, T. Endo, Y. Makita, *Cryst. Growth Des.* **2019**, *19*, 4162.
[35] H. Li, S. Guo, H. Zhou, *Energy Storage Mater.* **2023**, *56*, 227.
[36] B. Wang, R. Zheng, W. Yang, X. Han, C. Hou, Q. Zhang, Y. Li, K. Li, H. Wang, *Adv. Funct. Mater.* **2022**, *32*, 2112693.
[37] H. Yu, D. Chen, Q. Li, C. Yan, Z. Jiang, L. Zhou, W. Wei, J. Ma, X. Ji, Y. Chen, L. Chen, *Adv. Energy Mater.* **2023**, *13*, 2300550.
[38] Q. Gou, H. Luo, Q. Zhang, J. Deng, R. Zhao, O. Odunmbaku, L. Wang, L. Li, Y. Zheng, J. Li, D. Chao, M. Li, *Small* **2023**, *19*, 2207502.
[39] W. Han, L. Xiong, M. Wang, W. Seo, Y. Liu, S. T. U. Din, W. Yang, G. Liu, *Chem. Eng. J.* **2022**, *442*, 136247.
[40] S. Zhou, Y. Wang, H. Lu, Y. Zhang, C. Fu, I. Usman, Z. Liu, M. Feng, G. Fang, X. Cao, S. Liang, A. Pan, *Adv. Funct. Mater.* **2021**, *31*, 2104361.
[41] X. Zhu, X. Li, M. L. K. Essandoh, J. Tan, Z. Cao, X. Zhang, P. Dong, P. M. Ajayan, M. Ye, J. Shen, *Energy Storage Mater.* **2022**, *50*, 243.
[42] R. Yao, L. Qian, G. Zhao, H. Zhu, T. Qin, C. Xiao, H. Lin, F. Kang, C. Zhi, C. Yang, *J. Mater. Chem.* **2023**, *11*, 1361.
[43] Y. Lin, Z. Mai, H. Liang, Y. Li, G. Yang, C. Wang, *Energy Environ. Sci.* **2023**, *16*, 687.
[44] H. Yu, D. Chen, X. Ni, P. Qing, C. Yan, W. Wei, J. Ma, X. Ji, Y. Chen, L. Chen, *Energy Environ. Sci.* **2023**, *16*, 2684.
[45] M. Peng, X. Tang, K. Xiao, T. Hu, K. Yuan, Y. Chen, *Angew. Chem., Int. Ed.* **2023**, *62*, 202302701.
[46] K. Guan, L. Tao, R. Yang, H. Zhang, N. Wang, H. Wan, J. Cui, J. Zhang, H. Wang, H. Wang, *Adv. Energy Mater.* **2022**, *12*, 2103557.
[47] H.-Y. Wu, X. Gu, P. H. Huang, C. Sun, H. Hu, Y. Zhong, C. Lai, *J. Mater. Chem.* **2021**, *9*, 7025.
[48] L. Zhang, L. Miao, W. Xin, H. Peng, Z. Yan, Z. Zhu, *Energy Storage Mater.* **2022**, *44*, 408.
[49] C. Li, G. Qu, X. Zhang, C. Wang, X. Xu, *Energy Environ. Mater.* **2023**, e12608.
[50] J. Wan, R. Wang, Z. Liu, L. Zhang, F. Liang, T. Zhou, S. Zhang, L. Zhang, Q. Lu, C. Zhang, *ACS Nano* **2023**, *17*, 1610.
[51] W. Xu, K. Zhao, W. Huo, Y. Wang, G. Yao, X. Gu, H. Cheng, L. Mai, C. Hu, X. Wang, *Nano Energy* **2019**, *6*, 275.
[52] J. Luo, L. Xu, Y. Zhou, T. Yan, Y. Shao, D. Yang, L. Zhang, Z. Xia, T. Wang, L. Zhang, *Angew. Chem., Int. Ed.* **2023**, *62*, e202302302.
[53] T. Zhou, Y. Mu, L. Chen, D. Li, W. Liu, C. Yang, S. Zhang, Q. Wang, P. Jiang, G. Ge, *Energy Storage Mater.* **2022**, *45*, 777.
[54] M. Zhang, H. Hua, P. Dai, Z. He, L. Han, P. Tang, J. Yang, P. Lin, Y. Zhang, D. Zhan, J. Chen, Y. Qiao, C. C. Li, J. Zhao, Y. Yang, *Adv. Mater.* **2023**, *35*, 2208630.